Journal of Advanced Research xxx (xxxx) xxx

Contents lists available at ScienceDirect

Journal of Advanced Research

journal homepage: www.elsevier.com/locate/jare

Modulation of the tumor microenvironment through BMAL1-LHX8 axis augments the sensitivity of ameloblastoma to vemurafenib

Shujin Li [a,e], Eun-Jung Kim [a], Hyun-Yi Kim [b], Takashi Muramatsu [c], Jun-Young Kim [d], Jin Hoo Park [d], Young-Soo Jung [d], Han-Sung Jung [a,*]

[a] Division in Anatomy and Developmental Biology, Department of Oral Biology, Taste Research Center, Oral Science Research Center, BK21 FOUR Project, Yonsei University College of Dentistry, Seoul, South Korea
[b] NGeneS Inc., Ansan-si, South Korea
[c] Department of Operative Dentistry, Cariology and Pulp Biology, Tokyo Dental College, Tokyo, Japan
[d] Department of Oral and Maxillofacial Surgery, Yonsei University College of Dentistry, Seoul, South Korea
[e] Current Address: Hospital of Stomatology, Guanghua School of Stomatology, Guangdong Provincial Key Laboratory of Stomatology, Sun Yat-sen University, Guangzhou 510055, China

HIGHLIGHTS

- The ameloblastoma-associated fibroblasts (AMF) exhibit precedence levels of matrix contractility and secretory activity, that collectively contribute to the formation of drug resistance niche.
- Tumor-stroma crosstalk exacerbating the dysregulation of molecular clock, which promoting the AMFs activation via *BMAL1-LHX8* signaling axis.
- Targeting the *BMAL1-LHX8* axis through small-molecular modulators elevates the sensitivity of ameloblastoma against vemurafenib.

GRAPHICAL ABSTRACT

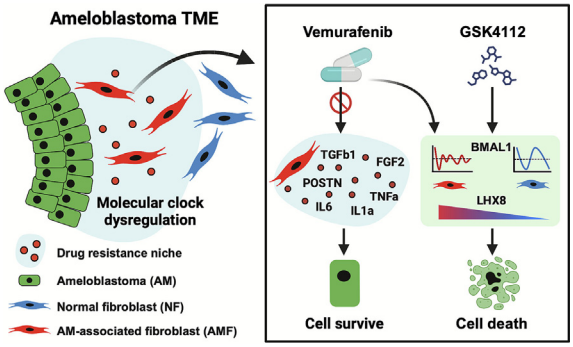

ARTICLE INFO

Article history:
Received 23 March 2025
Revised 7 November 2025
Accepted 28 November 2025
Available online xxxx

Keywords:
Ameloblastoma
Ameloblastoma-associated fibroblasts
BMAL1-LHX8
Vemurafenib

ABSTRACT

Introduction: Ameloblastoma (AM) frequently develops resistance to the BRAF inhibitor vemurafenib, primarily mediated by ameloblastoma-associated fibroblasts (AMFs). However, the potential contribution of the circadian clock in this resistance has not been explored.
Objectives: This study aimed to elucidate the role of the BMAL1-LHX8 axis during tumor-stroma crosstalk, and to investigate the therapeutic potential of targeting this axis to augment vemurafenib sensitivity for AM.
Methods: Patient-derived AM cells and AMFs were utilized to reconstruct the stroma-rich AM tumoroid *in-vitro* for recapitulating the tumor-stroma interplay and assessing the pharmacological effect of vemurafenib. Time-series RNA-sequencing, luciferase assays, and CRISPR/Cas9 gene editing were used to define the transcriptional landscape and the BMAL1-LHX8 regulatory network. The efficacy of combining the clock modulator GSK4112 with vemurafenib was assessed in stroma-rich AM tumoroids and cell line-based xenograft models.
Results: Patient-derived AMFs exhibit enhanced secretory activity, and elevated metabolic and contractile functions contribute to increased stromal stiffness through ECM remodeling in AM. Tumor-stroma crosstalk was recapitulated in stroma-rich AM tumoroid, which is evidenced by the dynamic alteration of normal fibroblasts (NFs) to AMF-like state. Transcriptomic profiling of stroma-rich tumoroids revealed severe disruption of the molecular clock and *LHX8* in AMFs. Functional studies demonstrated that *BMAL1*-driven *LHX8* expression promotes pro-tumorigenic AMF activities, including growth factor secretion and

* Corresponding author at: Department of Oral Biology, Yonsei University College of Dentistry, 50-1 Yonsei-ro, Seodaemun-gu, Seoul 03722, South Korea.
E-mail address: hsjung@yuhs.ac (H.-S. Jung).

https://doi.org/10.1016/j.jare.2025.11.069

Please cite this article as: S. Li, E.-J. Kim, H.-Y. Kim et al., Modulation of the tumor microenvironment through BMAL1-LHX8 axis augments the sensitivity of ameloblastoma to vemurafenib, Journal of Advanced Research, https://doi.org/10.1016/j.jare.2025.11.069

ECM remodeling. Critically, pharmacological inhibition of the BMAL1-LHX8 axis with GSK4112 potently sensitized AM to vemurafenib in both stroma-rich tumoroid and xenograft models.

Conclusion: Our findings reveal the role of the BMAL1-LHX8 axis in underlying AMF-mediated drug resistance in AM, and propose that the molecular clock modulation in tumor-stroma crosstalk represents a potential therapeutic avenue for ameloblastoma.

Introduction

Ameloblastoma (AM), the most prevalent odontogenic epithelial tumor in maxillofacial region, exhibits significant osteolytic potential and locally invasive growth. Surgical intervention remains the only curative treatment, it carries substantial recurrence risks. Recent Phase I trial data indicate that BRAF inhibition (vemurafenib) shows promising tumor-suppressive effects in unresectable AM cases [1]. Nevertheless, the vemurafenib is hampered by inconsistent therapeutic responses and toxicity profiles. Compounding this challenge, BRAF inhibitors trigger cancer-associated fibroblast (CAF) activation—a mechanism known to drive tumor cell resistance via periostin secretion in melanoma [2]. Our prior work identified a CAF-like population (ameloblastoma-associated fibroblasts, AMFs) at AM invasive fronts, characterized by elevated secretory and extracellular matrix (ECM) remodeling activities [3]. This led to the proposal that AMF activation might be a crucial factor influencing the therapeutic effectiveness of vemurafenib against AM.

Circadian rhythm, an evolutionarily conserved biological phenomenon, synchronizes the rhythmicity of physiological, behavioral, and biochemical functions throughout the body, generated by an endogenous clock system [4]. Molecularly, the circadian clock comprises a series of transcription–translation feedback loops governed by core clock genes [5]. Accumulating evidence indicates that dysregulation of circadian clock genes not only promotes the tumorigenesis but also shapes the dynamics of tumor microenvironment (TME) [6–9]. Consequently, deciphering clock-mediated tumor-TME symbiosis presents a strategic avenue for developing novel anticancer therapies.

Brain and muscle arnt-like protein 1 (*BMAL1*) is a master gene of circadian clock, regulates essential processes in oral development and pathology. Transcriptional dysregulation of *BMAL1* perturbates the mandibular bone homeostasis [10], disrupts the enamel formation [11], and elevates the chemoresistance in oral cancer [12]. Nevertheless, the role of *BMAL1* in ameloblastoma has not been studied. Importantly, emerging evidence positions the *BMAL1* as a direct upstream modulator of the *MAPK* pathway. In colorectal cancer, *BMAL1* overexpression has been shown to activate the MAPK cascade, specifically increasing phosphorylation of *RAF*, *MEK*, *ERK*, and *JNK*, thereby driving oncogenic phenotypes [13]. Furthermore, *BMAL1* can differentially regulate *MAPK* family members, as it also demonstrates the capacity to suppress *MAPK-p38* phosphorylation [14]. Given that *BRAF* is a key initiator of the *RAF-MEK-ERK* axis, these findings establish a compelling mechanistic foundation for role of *BMAL1* in influencing *BRAF/MAPK* signaling output.

LIM homeobox 8 (*LHX8*) is a key developmental transcription factor with a highly tissue-restricted expression pattern, found primarily in craniofacial mesenchymal lineages [15], neural tissues [16], and oocytes [17], where it regulates cell fate determination, proliferation, and differentiation [18]. Dysregulation of *LHX8* has been linked to pathologies including cleft palate [19], Alzheimer's disease [20], and tumorigenesis—notably in cervical cancer and odontogenic tumors [21,22]. Importantly, bioinformatic analyses suggest that the promotor region of *LHX8* contains binding sites for *BMAL1* [15], raising the possibility of direct transcriptional regulation by *BMAL1*. Consequently, we hypothesized that the BMAL1-LHX8 axis could be a critical determinant of cellular response to *BRAF*-targeted therapies like vemurafenib.

In this study, we investigated the roles of BMAL1-LHX8 axis during the crosstalk between AM and its TME, and explored the potential as a therapeutic target. This offers a new and innovative chronobiological perspective on this disease.

Results

Comprehensive analysis and characterization of AMFs

We performed a comprehensive histological analysis on 17 conventional AM samples. Masson's trichrome staining revealed that collagen bundles in the AM stroma were thicker, more aligned, and more abundant (bluish-stained) compared to those in normal adjacent tissues (NATs) (Fig. 1A). To further define these regions, we annotated the tumor and stroma using immunohistochemistry for a panel of markers related to epithelial (E-cadherin, CK14, CK19), mesenchymal (Vimentin, FAP, α-SMA), vascular (CD146), and immune cells (CD8a, CD68, CD56), followed by histological comparison to NATs (Fig. 1B and Fig. S1A). AMFs constituted a substantial portion of the cells in the AM tumor microenvironment (Fig. 1C). The TME displayed considerable cellular heterogeneity, featuring a fibrotic stroma infiltrated by blood vessels and immune cells.

To gain deeper insight into the characteristics of AMF, we isolated stromal cells from invasive front of AM biopsies and confirmed the fibroblast identity through positive staining for vimentin and α-SMA (Fig. 1D). Elongated shape of AMFs was substantially observed when it compared to the normal fibroblasts (NFs, derived from NATs, Fig. S1B). AMFs also exhibited significantly higher mitochondrial expression, as estimated by MitoTracker® probe (Fig. 1E). Functional assays demonstrated that AMFs possess greater contractile ability. In a collagen gel contraction assay [23], matrices embedded with AMFs shrank significantly more than those with NFs over 12 days, as quantified by the shrinking area and confirmed with picrosirius red staining (Fig. 1F, G). Furthermore, a co-culture system of AM cells with AMFs showed significant upregulation of mRNA for key growth factors (POSTN, TGFB1, FGF2) and cytokines (IL1A, IL6, TNFA) compared to normal controls (Fig. 1H, I).

Collectively, these results indicate that AMFs are hyperactive, enlarged cells with elevated metabolic and contractile functions. Their enhanced secretory activity likely contributes to increased stromal stiffness through ECM remodeling in AM.

Reconstructing AM-AMFs interaction within stroma-rich tumoroid

To investigate fibroblast transformation within tumor-stroma interactions under controlled settings, we developed an advanced stroma-rich tumoroid co-culture system, building upon our previous model [24]. In this system, AM tumoroids were reconstituted with NFs or AMFs in Matrigel® and monitored for 7 or 14 days

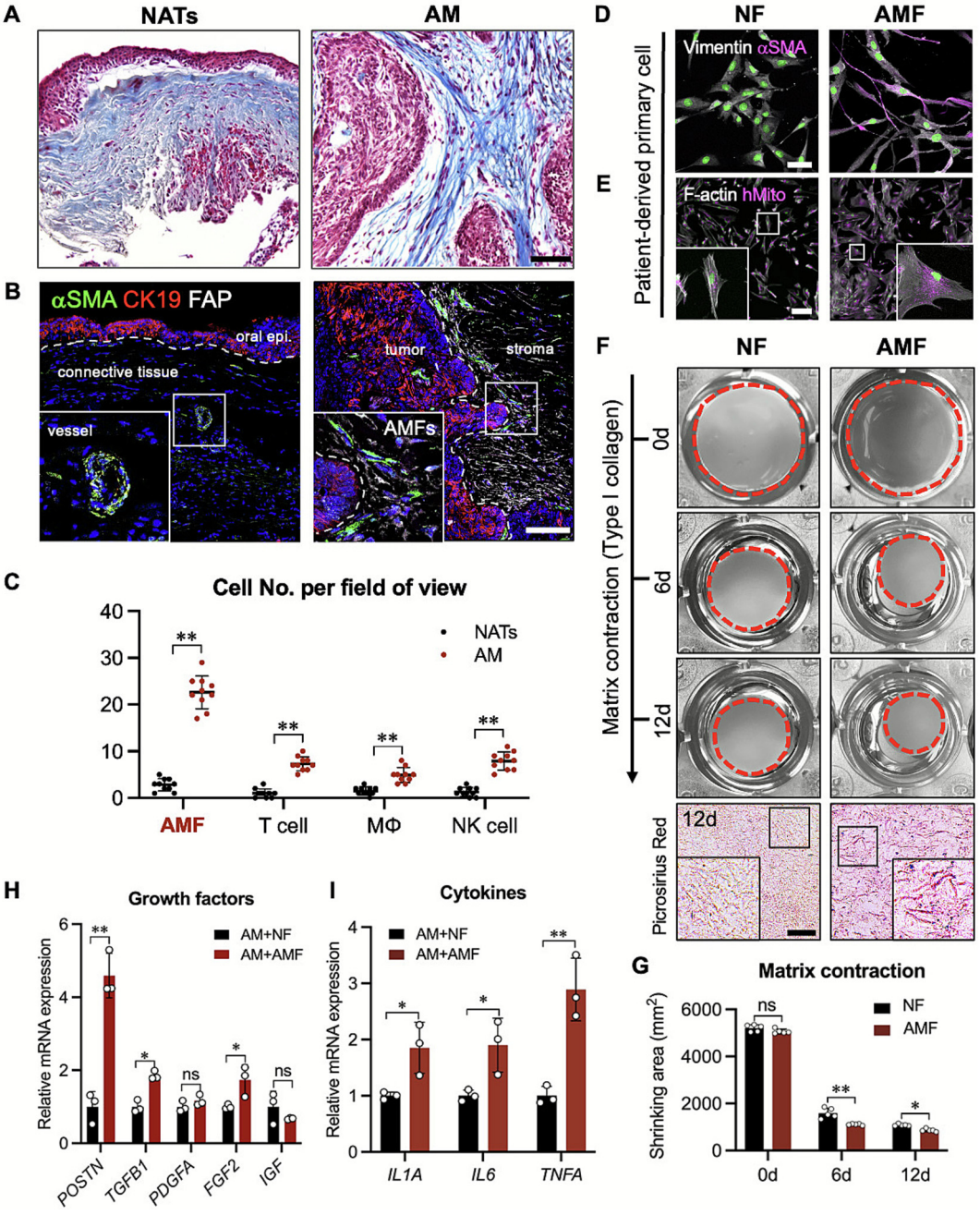

Fig. 1. Significance of cellular composition in tumor microenvironment of ameloblastoma. (A) Masson's trichrome staining for NATs and AM. (B) Immunohistochemistry staining for α-SMA CK19 and FAP. (C) Quantification of the cellular components in the TME of AM. (D, E) Immunocytochemistry staining for vimentin, α-SMA, F-actin, and mitochondria (MitoTracker® probe) in patient sample-derived stromal cells. (F) Stereoscopic images of NFs- or AMFs-embedded type I collagen gel at day 0, day 6 and day 12. Picrosirius red staining performed with shrieked collagen gel at day 12. (G) Quantification of shrinking area of NFs- or AMFs-embedded collagen gels at 0, 6, and 12 days. (H) Relative mRNA expressions of *POSTN*, *TGFB1*, *PDGFA*, *FGF2*, and *IGF* in NFs or AMFs co-cultured with AM tumoroids for 7 days. (I) Relative mRNA expressions of *IL1A*, *IL6*, *and TNFA* in NFs or AMFs co-cultured with AM tumoroids for 7 days. Data were shown as mean ± SEM, one-way ANOVA followed Šídák's multiple comparisons test was used in C, G, H, I. (C, n = 10, G, n = 5, H and I, n = 3; ns, not significant; $^{**}p < 0.01$, $^{*}p < 0.05$). Scale bars: A, B, D, F (Picrosirius red), 100 μm; E, 50 μm. White dotted line indicates the interface between the tumor and stromal tissue. Nuclear stained with TO-PRO-3 (TP3).

(Fig. 2A). By day 7, synaptic connections were observed between AM tumoroids and the surrounding AMFs (Fig. 2B). This cellular crosstalk is a fundamental driver of intratumoral diversity, facilitated by a dynamic paracrine loop involving growth factors, cytokines, and metabolic enzymes [25]. End-point analysis on day 14 revealed that vimentin-positive stromal cells had infiltrated the core of AM tumoroids (Fig. 2C). The presence of FAP-positive cells in both the AM + NF and AM + AMF co-cultures suggests that NFs can transform into an AMF-like phenotype after interacting with AM cells. Proliferation, indicated by PCNA-positive cells, was significantly higher in the AM + AMF group than in AM + NF, underscoring the role of AMF paracrine signaling in promoting active cell division. We also found intense expression of glycogen phosphorylase (PYGB), an enzyme linked to glycogen mobilization in several cancers [26–29], in the AM + AMF group compared to AM + NF.

To dynamically track these interactions, AM cells were transfected with an mCherry fluorescent protein plasmid before tumoroid formation. Time-lapse imaging over the 14-day culture period showed little change in tumoroid growth or stromal cell migration

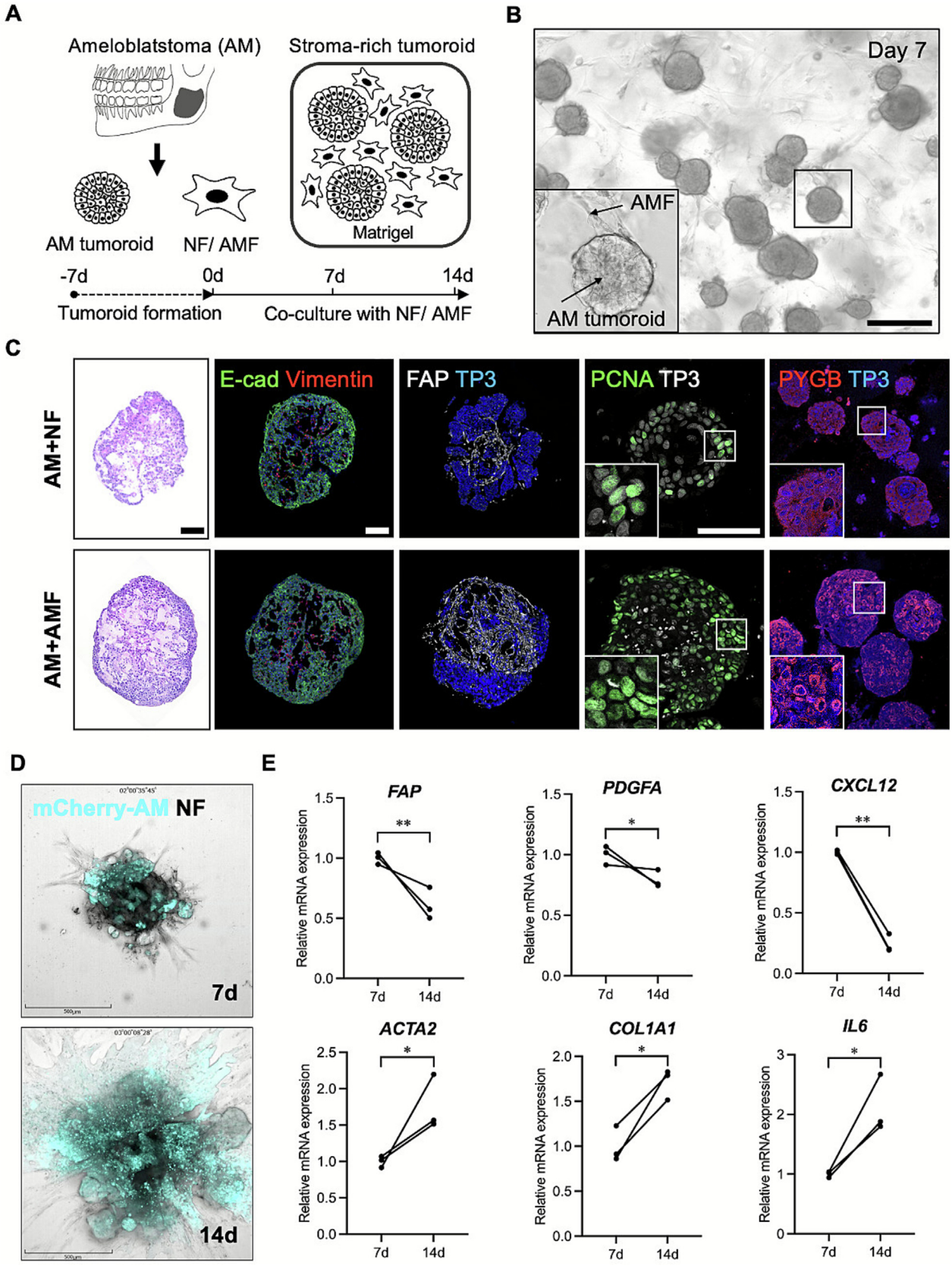

Fig. 2. Establishment and characterization of stromal-rich AM tumoroids. (A) Schematic illustration and culture schedule for establishing stromal-rich tumoroids. (B) DIC images of stromal-rich tumoroids following co-culture with AMFs for 7 days. A representative image (magnified) of the interaction between the AM tumoroid and AMFs. (C) Histological analysis of the AM + NF or AM + AMF group at the co-culture day 7. H&E and immunohistochemistry staining of E-cadherin, vimentin, FAP, PCNA, and PYGB. (D) Representative time-lapse images of the AM + NF group at co-culture day 7 and 14. AM tumoroids were tagged with mCherry. (E) Relative mRNA expression of *FAP*, *PDGFA*, *CXCL12*, *ACTA2*, *COL1A1*, and *IL6* in samples from the co-culture day 7 and 14 groups. Data were shown as mean ± SEM, Unpaired two-tailed *t*-test was used in E. (n = 3 per group; $^{**}p < 0.01$, $^{*}p < 0.05$). Scale bars: B, 200 μm; C, 100 μm; D, 500 μm. Nuclear stained with TO-PRO-3 (TP3).

until day 7. However, by day 14, we observed pronounced radial movement of NFs into the extracellular matrix and aggressive expansion of the tumoroids (Fig. 2D). Molecular analysis identified distinct gene expression profiles between co-culture day 7 (7d) and day 14 (14d). Early time points (7d) were marked by elevated expression of *FAP*, *PDGFA*, and *CXCL12*, while later time points (14d) showed strong upregulation of *ACTA2*, *COL1A1*, and *IL6* (Fig. 2E). These results indicate that day 7 represents a critical transition point for phenotypic alteration of stromal cells in this model.

Tumor-stroma crosstalk exacerbated the perturbation of molecular clock in fibroblasts

To explore the transitional dynamics of stromal cell plasticity, we analyzed dexamethasone (Dex)-synchronized, stroma-rich AM tumoroids (co-cultures of AM with NFs or AMFs) harvested at 8-hour intervals over 48 h for RNA-sequencing. Principal component analysis (PCA) and a transcriptomic heatmap revealed distinct clustering, with a clear separation between the AM + NF (black dots) and AM + AMF (red dots) group. Within the AM + AMF cluster, samples from different time points were well-separated, whereas they remained closely grouped in the AM + NF cluster, indicating greater transcriptional variability over time in the former (Fig. 3A and Fig. S3A). Gene ontology (GO) analysis of differentially expressed genes (DEGs) showed significant upregulation of terms related to ECM remodeling, secretory activity, and metabolic processes in the AM + AMF group compared to the AM + NF group (Fig. 3B). Notably, expression of 24 core clock genes was also elevated in the AM + AMF group (Fig. 3C). Consistently, the upregulated expression of *BMAL1* (Fig. S3B), and dysregulation of circadian clock genes (including *BMAL1*, *BMAL2*, *CLOCK*, *PER1*, *PER2*, *CRY1*, *RORA*, *RORC*, *REV-ERB*, and *NFIL3*) were confirmed in AM samples derived from patients (Fig. S3C). Dysregulation of the core clock genes were pronounced in AM + AMF cultures, where oscillation of clock-controlled genes was markedly disrupted compared to the robust 24-hour rhythmicity observed in AM + NF groups (Fig. 3D). Rhythmic expression was maintained in only 2.20 % of genes in AM + AMF versus 4.59 % in AM + NF (Fig. S3D). *LHX8*, a transcription factor critical for craniofacial connective tissue development, was among the top 10 upregulated genes from the set whose rhythmic expression was disrupted (Fig. 3E). This upregulation was confirmed in the stromal regions of patient-derived AM samples compared to NATs (Fig. S3E).

To further confirm the effect of tumor-stromal interactions on intrinsic cellular rhythms, we examined *BMAL1* expression at various time points in NFs co-cultured with AM-1 cells for 7 and 14 days. *BMAL1* showed rhythmic expression during 32 h period of time, peaking at 16–24 h in 7d co-cultured group. Following 14 days of co-culture, however, *BMAL1* was constitutively expressed in the nucleus throughout the time course (Fig. 3F), with loss of rhythmicity. It was also confirmed at the mRNA level for *BMAL1, PER2* (Fig. 3G).

Together, these results demonstrate that prolonged tumor-stroma interaction exacerbates dysregulation of molecular clock in fibroblasts, promoting their transition to a tumor-supportive state. This process appears driven by core clock gene – *BMAL1* and strongly correlative with aberrant *LHX8* upregulation.

Dysregulation of molecular clock promotes the AMF activation via BMAL1-LHX8 axis

To determine whether dysregulation of molecular clock drives the acquisition of tumor-supportive functions in fibroblasts through BMAL1-LHX8 pathway, we first assessed the transcriptional activity of BMAL1 in AMFs. NFs and AMFs were transfected with *PER2*::Luc (790 bp) reporter plasmid and monitored bioluminescence over 48 h. Notably, a significantly enhanced oscillation and disrupted rhythmicity of PER2-driven luminescence was observed in AMFs compared to NFs (Fig. 4A). To explore the potential regulatory link between *BMAL1* and *LHX8*, we employed siRNA-mediated *BMAL1* knockdown, and verified the reduced mRNA expression in NFs (Fig. S4A). This intervention resulted in diminished nuclear localization of both BMAL1 and LHX8 in NFs following 7 days of exposure to AM tumoroids (Fig. 4B). Notably, the nucleonic expression of the BMAL1 and LHX8 were reduced by the knockdown of *BMAL1* in NFs which co-culture with AM tumoroids for 7 days. Similarly, the protein expression of BMAL1, LHX8, FAP, and POSTN in AMFs were markedly reduced in siBMAL1 group (Fig. 4C). Corresponding experiments showed that *BMAL1* knockdown substantially reduced protein levels of BMAL1, LHX8, and FAP in NFs (Fig. 4C and S4F).

To elucidate the potential regulatory relationship between *BMAL1* and *LHX8*, we examined the temporal mRNA expression of *LHX8* in synchronized AMFs, revealing a rhythmic pattern and a specific phase relationship with *BMAL1*. We noticed without interaction with tumor, the BMAL1 kept the rhythmical expression pattern during the 48-hours monitoring in AMFs cells. The *LHX8* expression showed relatively damped and delayed phase when compared with *BMAL1* (Fig. S4C). Using CRISPR/Cas9-generated *BMAL1* knockout (KO) fibroblasts (Fig. S4B) co-cultured with AM tumoroids for 14 days, we observed significantly decreased mRNA expression of *LHX8* and core clock genes (*PER1, PER2, CRY1, RORA,* and *REV-ERB*) compared to wild-type (WT) cells (Fig. 4D, E). Furthermore, *BMAL1* ablation downregulated expression of pivotal growth factors (*POSTN, TGFB1, PDGFA, FGF2*) and extracellular matrix remodeling components (*COL1A1, ACTA2, FAP, LOXL2, CCN4, MMP9*) (Fig. 4F, G). To explore the potential correlation between the activation of the BMAL1-LHX8 axis in AMFs and the cellular response to vemurafenib, the spatial expression pattern of BMAL1 and LHX8 at cellular level were investigated with immunofluorescence staining. We observed that treatment with Vemurafenib (20 μM, 6 h) significantly enhanced the nuclear co-localization of BMAL1 and LHX8 compared to the control group (Fig. S4D, E), providing interim mechanistic insight.

These findings indicate that tumor-stroma crosstalk induces dysregulation of molecular clock in fibroblasts, driving their transition to a tumor-promoting state. We consider the BMAL1-LHX8 axis could potentially involve in this transition, that coordinated the formation of drug resistance niche in TME of ameloblastoma (Fig. 4H).

Tuning the clock augments the sensitivity of ameloblastoma against vemurafenib

The acquisition of drug resistance in cancer is closely related to activated fibroblasts in TME, which protect cancer cells against drug-induced apoptosis by producing soluble cytokines, chemokines, growth factors, and exosomes [30–32]. Since the secretion activity of AMFs were significantly elevated by *BMAL1-LXH8* axis, we hypothesized that inhibiting this axis might prevent NFs from acquiring AMF-like characteristics, thereby sensitizing tumors to treatment. Herein, we developed a sequential therapeutic approach: first modulating rhythmicity of molecular clock with GSK4112 (a REV-ERB agonist that inhibit *BMAL1* expression), followed by treatment with the vemurafenib/ PLX4032 (Fig. 5A). The dose–response curves for the AM, AM + NFs, and AM + AMFs groups in response to PLX4032 after 24 h were analyzed using the CCK-8 cytotoxicity assay. The IC_{50} values obtained were 10.34 μM for the AM group, 17.72 μM for the AM + NFs group, and 25.38 μM, for the AM + AMFs group. Notably, the dose–re-

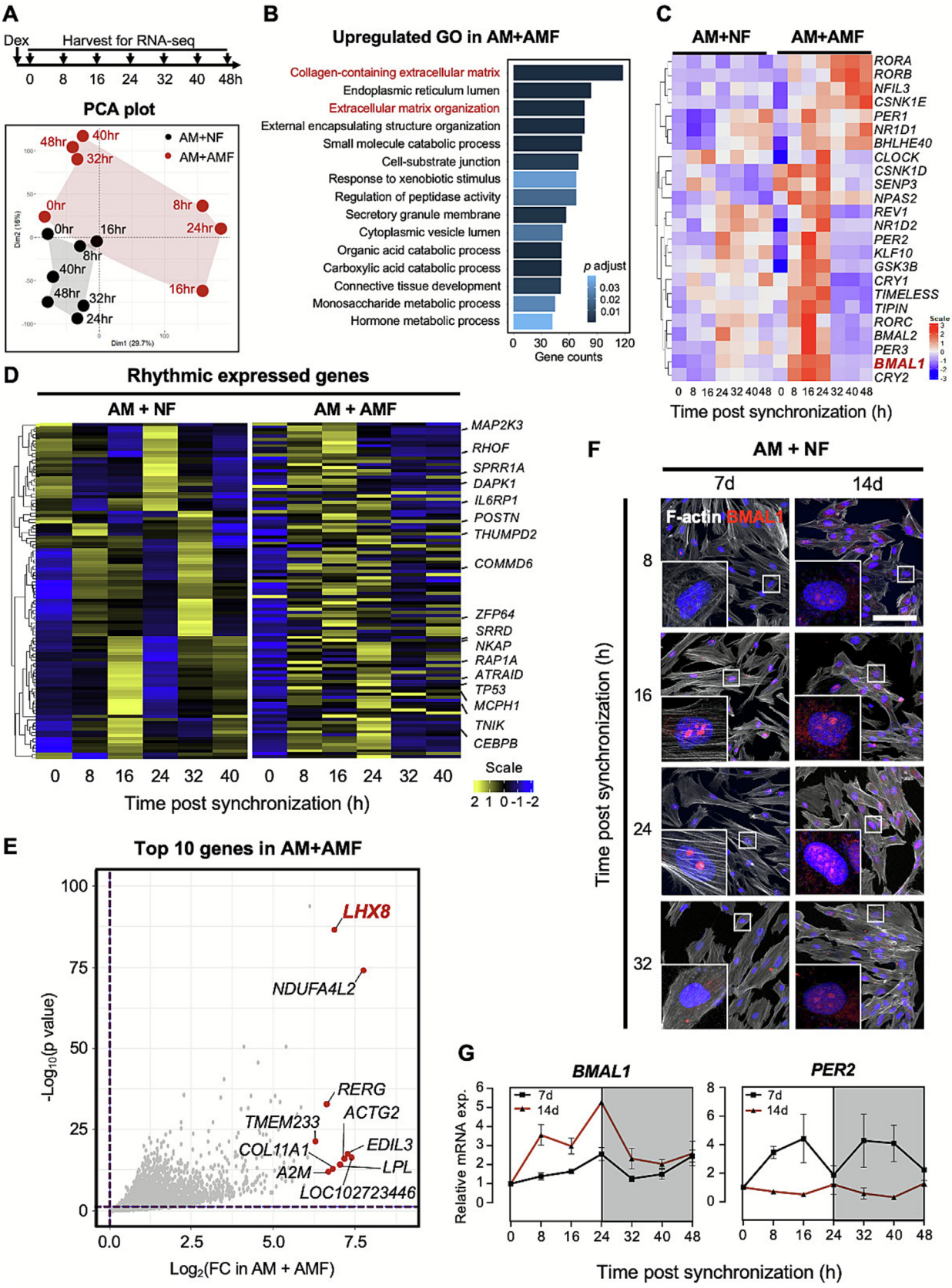
A
Dex
Harvest for RNA-seq
0 8 16 24 32 40 48h
PCA plot
AM+NF
AM+AMF
B
Upregulated GO in AM+AMF
Collagen-containing extracellular matrix
Endoplasmic reticulum lumen
Extracellular matrix organization
External encapsulating structure organization
Small molecule catabolic process
Cell-substrate junction
Response to xenobiotic stimulus
Regulation of peptidase activity
Secretory granule membrane
Cytoplasmic vesicle lumen
Organic acid catabolic process
Carboxylic acid catabolic process
Connective tissue development
Monosaccharide metabolic process
Hormone metabolic process
p adjust
0.03
0.02
0.01
Gene counts
C
AM+NF
AM+AMF
RORA
RORB
NFIL3
CSNK1E
PER1
NR1D1
BHLHE40
CLOCK
CSNK1D
SENP3
NPAS2
REV1
NR1D2
PER2
KLF10
GSK3B
CRY1
TIMELESS
TIPIN
RORC
BMAL2
PER3
BMAL1
CRY2
Scale
Time post synchronization (h)
D
Rhythmic expressed genes
AM + NF
AM + AMF
MAP2K3
RHOF
SPRR1A
DAPK1
IL6RP1
POSTN
THUMPD2
COMMD6
ZFP64
SRRD
NKAP
RAP1A
ATRAID
TP53
MCPH1
TNIK
CEBPB
Scale
Time post synchronization (h)
E
Top 10 genes in AM+AMF
LHX8
NDUFA4L2
RERG
ACTG2
TMEM233
COL11A1
EDIL3
A2M
LPL
LOC102723446
-Log10(p value)
Log2(FC in AM + AMF)
F
AM + NF
7d
14d
F-actin BMAL1
Time post synchronization (h)
G
BMAL1
PER2
7d
14d
Relative mRNA exp.
Time post synchronization (h)

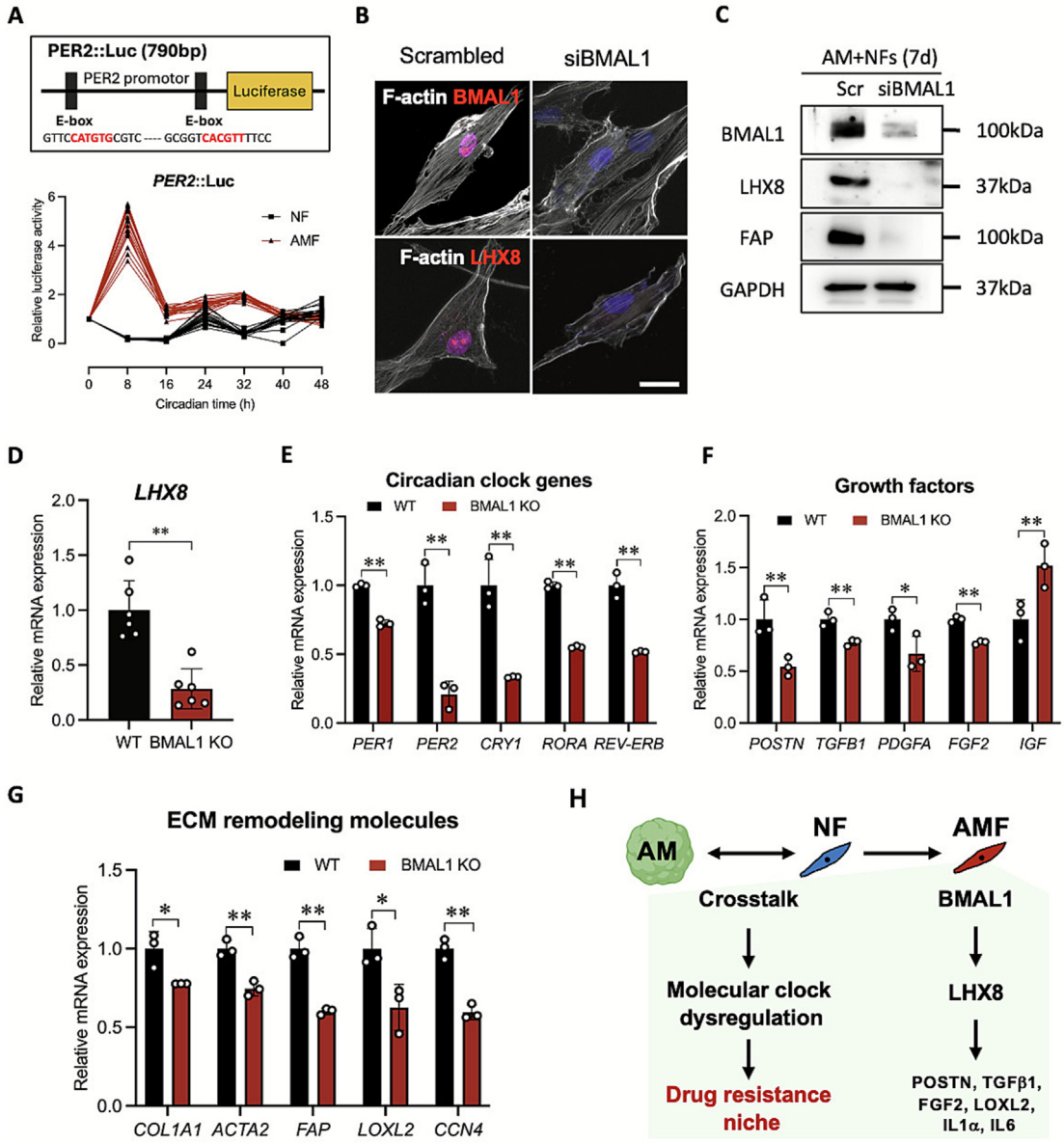

Fig. 4. Correlation between dysregulation of BMAL1 and tumor-supportive activities in AMFs. (A) The luciferase sequences were inserted into the promotor region of *PER2*. Translational activity of *BMAL1* was monitored via PER2::Luc reporter plasmid transfected NFs or AMFs (n = 18) for 48 h after Dex-induced synchronization. (B) The siRNA-mediated knockdown of *BMAL1* in NFs decreased nuclear accumulation of both BMAL1 and LHX8 proteins in NFs following 7 days of exposure to AM tumoroids. Scale bar: H, 25 μm. Nuclear stained with TO-PRO-3 (TP3). (C) Western blot assay for BMAL1, LHX8, FAP and GAPDH in the *BMAL1* knockdown NFs that following 7 days of exposure to AM tumoroids. (D-G) Relative mRNA expression of *LHX8, PER1, PER2, CRY1, RORA, REV-ERB, POSTN, TGFB1, PDGFA, FGF2, IGF, COL1A1, ACTA2, FAP, LOXL2* and *CCN4* in the *BMAL1* knockout NFs that following 7 days of exposure to AM tumoroids. Data were shown as mean ± SEM, one-way ANOVA followed Šídák's multiple comparisons test was used in D-G (D, n = 6, E-G, n = 3; $^{**}p < 0.01$, $^{*}p < 0.05$). (H) Schematic diagram of correlation between circadian perturbation and increased tumor supportive activity.

sponse curve for the AM + AMFs group (represented by the red curve) shifted horizontally to the right, indicating an increase in drug resistance to PLX4032 due to the influence of AMFs (Fig. 5B).

From a panel of circadian-modulating compounds (KL001, KS15, GSK4112, and SR1078), GSK4112 most effectively inhibited BMAL1-LHX8 signaling in the stroma-rich tumoroid system

Fig. 3. Transcriptomic analysis in stromal-rich AM tumoroids via time-series RNA-seq. (A) Sampling schedule and PCA of transcriptomes from stromal-rich AM tumoroids. (B) Top 15 of upregulated GO terms in the AM + AMF group consisting of genes related to the ECM remodeling, extracellular secretion and metabolism. (C) Heatmap of genes consisting of the GO terms related to pattern of molecular clock. (D) Heatmap showing the median-normalized gene expression (Exp. / Med.) ordered by the MetaCycle phase, depicting all significant rhythmically expressed genes identified in the AM + NF group. The same genes appear arrhythmical expression in AM + AMF group. (E) Volcano plots of DEGs of AM + AMF. Fold changes are shown for all DEGs (|fold change| > 1 and *p*-value < 0.05), as red dots indicated the top 10 rated genes. Vertical dashed lines indicate + 1-fold changes. A horizontal dashed line indicates a *p*-value of 0.05. (F) The nuclear expression of *BMAL1* in NFs co-cultured with AM tumoroids for 7 or 14 days at the time post-synchronization of 8, 16, 24, and 32 h. (G) Core clock gene *BMAL1* and *PER2* expression over the clock cycle in NFs co-cultured with AM tumoroids for 7 or 14 days after DEX-induced synchronization. Student's *t*-test comparing levels of gene expression of day 7 vs. day 14 at individual circadian times. (n = 3).

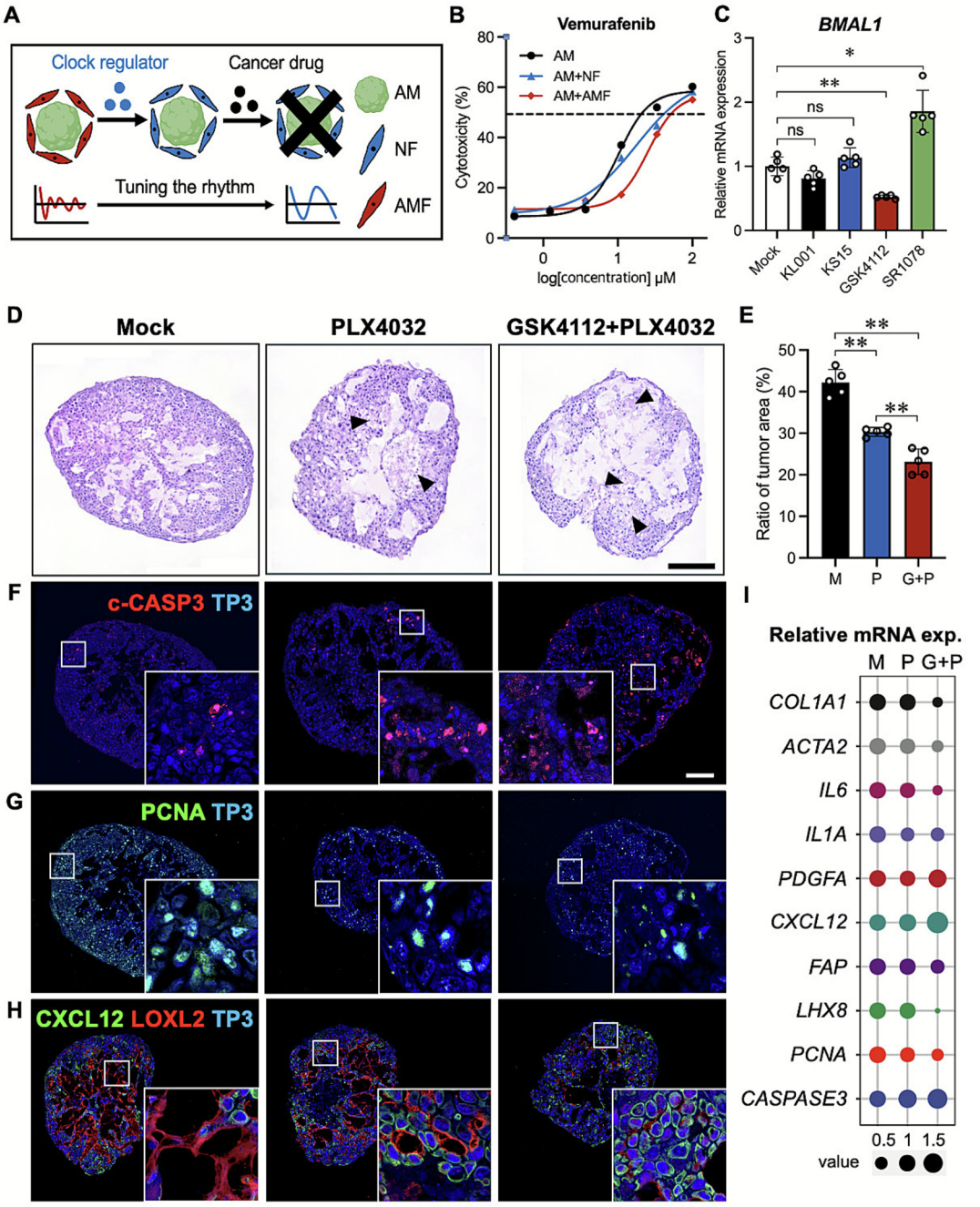

Fig. 5. Pharmacological modulation of molecular clock augments the anti-tumor efficacy of vemurafenib. (A) Schematic diagram of combined administration strategy for clock gene modulator and cancer drug. The anti-tumor efficacy is estimated in stromal-rich tumoroid model. (B) Dose-response curve of AM only, AM + NF and AM + AMF group, to PLX4032 (BRAF inhibitor) for 24 h determined by the CCK-8® cytotoxicity assay. Assays were performed according to the kit protocol in triplicate. The determined IC_{50} are 10.34, 17.72, 25.38 μM. (C) Effect of small-molecule modulators targeting *BMAL1*. (D) H&E staining of stromal-rich tumoroids in Mock, PLX4032, and GSK4112 + PLX4032 groups. Arrowheads indicates the apoptotic/ necrotic areas in the field of view. (E) Quantification of ratio of tumor area of stromal-rich tumoroids. (F) Cleaved-caspase3 staining for apoptotic cells in each group. (G) PCNA staining for proliferating cells in stromal-rich tumoroids in each group. (H) CXCL12 and LOXL2 expression in stromal-rich tumoroids. (I) Relative mRNA expression of *COL1A1*, *ACTA2*, *IL6*, *IL1A*, *PDGFA*, *CXCL12*, *FAP*, *LHX8*, *PCNA* and *Caspase3* in Mock, PLX4032 only, and GSK4112 + PLX4032 treatment groups. Scale bar: D, 200 μm; F-H, 100 μm. Nuclear stained with TO-PRO-3 (TP3). Data were shown as mean ± SEM, one-way ANOVA followed Tukey's multiple comparisons test was used in C, E (n = 5 per group; ns, not significant; **p < 0.01). M, Mock; P, PLX4032; G + P, GSK4112 + PLX4032.

(Fig. 5C). The relative inhibition was calculated across multiple cell types at 12 h-post administration with a range of GSK4112 concentrations (0–100 μM). AMF and AM cells (AM-1) were most sensitive, reaching IC_{50} sooner than normal epithelial cell (HEK293T), NFs, and endothelial cells (HUVEC), indicating a potential therapeutic window to minimize off-target effects (Fig. S5A). To further eliminate concerns regarding the off-target effects of GSK4112 in this study, we confirmed the mRNA expression of *PGC1A*, an established transcriptional target of *REV-ERBα*, was significantly repressed at the presence of 10 μM GSK4112 (Fig. S5B). Furthermore, the impact of timing of drug administration is vital for a chronotherapeutic claim. We accessed the mRNA expression of *BMAL1*, *LHX8* and *POSTN* in AMFs after administrating GSK4112 at different circadian time point (CT8, CT16, CT24). Our results

indicating that treatment at circadian time CT16 induced the strongest suppression of *BMAL1*, *LHX8*, and *POSTN*, underscoring the chronotherapeutic potential of this approach (Fig. S5C).

Subsequent combination treatment with GSK4112 and PLX4032 (G + P) significantly enhanced antitumor effects. Although H&E staining showed no major size differences between groups, cellularity was markedly reduced and apoptotic regions (black arrowheads, identified by nuclear morphology [33] were expanded in the G + P group (Fig. 5D, S5D). Further analyses confirmed therapeutic efficacy: tumor area was reduced (Fig. 5E), apoptosis was increased as indicated by cleaved caspase-3 (Fig. 5F, S5E), and proliferation was suppressed as indicated by PCNA (Fig. 5G, S5F) in the combination group. Moreover, expression of CXCL12 increased [34] while LOXL2 decreased [3], suggesting a reversal of AMF activation (Fig. 5H, S5G). The mRNA analysis corroborated these findings, showing downregulation of profibrotic (*COL1A1*, *ACTA2*, *FAP*), inflammatory (*IL6*, *IL1A*), and proliferative (*PCNA*) genes, and upregulation of *PDGFA*, *CXCL12*, and *CASPASE3* in the G + P group (Fig. 5I).

These results demonstrate that targeting the BMAL1-LHX8 axis with GSK4112 attenuates AMF-like activation, and restores sensitivity to targeted therapy, offering a promising avenue to overcome stroma-mediated drug resistance in AM.

Pharmacological inhibition of BMAL1-LHX8 axis with GSK4112 enhance the anti-tumor efficacy of vemurafenib

Building upon previous studies [35,36], we developed an AM-1 cell line xenograft mouse model to evaluate the therapeutic potential of circadian clock modulation in AM. Tumor-bearing mice were randomized into three treatment groups: mock (M), PLX4032 (P), and GSK4112 + PLX4032 (G + P), receiving intraperitoneal injections according to the schedule (Fig. 6A). Tumor volume increased steadily in both the M and P groups throughout the entire monitoring period. In contrast, the G + P group exhibited a significant reduction in tumor growth beginning on day 6 (Fig. 6B). Although a decrease in body weight was observed in the G + P group—potentially reflecting systemic metabolic effects of GSK4112—this group demonstrated a superior tumor growth inhibition index compared to the P group by day 4 (Fig. 6C, D). These results highlight the limited efficacy of vemurafenib (PLX4032) monotherapy and underscore the potential of circadian regulation to enhance its antitumor activity.

Molecular analysis of freshly dissected tumor masses showed marked downregulation of AMF-associated genes (*LHX8, FAP, COL1A1, ACTA2, LOXL2,* and *CXCL12*) in the G + P group compared to the M and P group (Fig. 6E). Stereoscopic imaging revealed abundant vascular bundles on tumors from the M group, which were reduced in both treatment groups (Fig. 6F). Histological examination via H&E staining indicated decreased cellularity and increased apoptotic regions in G + P-treated tumors (Fig. 6G). CD31 staining showed well-formed vascular structures in the M group, while endothelial cell networks appeared disrupted in treatment groups (Fig. 6H). Immunostaining further confirmed reduced proliferation (PCNA) and increased apoptosis (cleaved caspase-3) in the G + P group (Fig. 6I). Additionally, stromal AMFs, labeled with α-SMA and FAP, were significantly reduced following combination therapy (Fig. 6J), indicating suppression of tumor-supportive stromal activation. Western blot analysis demonstrated inhibition of pERK1/2, confirming effective MAPK pathway suppression by PLX4032, particularly in the G + P group. LHX8 expression correlated positively with proliferation (PCNA) and negatively with apoptosis (c-CASP3), supporting its role as a key mediator of AMF functionality and treatment resistance (Fig. 6K, S6A).

To mitigate potential systemic effects of GSK4112 on the central circadian clock, we developed a localized delivery system using poly(lactic-co-glycolic acid) (PLGA) nanoparticles encapsulated with GSK4112 and tagged with rhodamine (Fig. 6L, S6D). In co-culture experiments, neither PLX4032 alone (Fig. 6M) nor rhodamine-tagged PLGA nanoparticles (Fig. 6N) significantly affected tumor cells. However, GSK4112-loaded nanoparticles (GSK4112-Rho-PLGA) primed on AMFs dramatically enhanced anti-tumor efficacy when co-cultured with AM-1 cells (Fig. 6O).

These findings demonstrate that nanoparticle-mediated delivery of GSK4112 effectively targets the tumor microenvironment and potentiates PLX4032 efficacy by suppressing AMF activation, offering a promising chronotherapeutic strategy for ameloblastoma while minimizing systemic circadian disruption.

Discussion

The nature of the association between cancer and circadian rhythm remains a topic of debate. For instance, circadian rhythms are abrogated in many types of cancers [37,38], and that the loss of circadian regulation caused by genetic or environmental changes may even be linked to the onset or progression of cancer [39]. For instance, disruption of circadian clock can trigger an immunosuppressive TME by augmenting the abundance of tumor-associated macrophages and regulatory T cells [40]. Conversely, several malignancies retain the daily oscillations of gene expression driven by the functional circadian clock [41,42]. In the present study, we identified that AM cells induce transcriptional perturbation of *BMAL1* in neighboring fibroblasts, suggesting that a loss of circadian precision is a potential initiating factor.

The activation of NFs into a tumor-promoting, activated state (AMFs in this context) is a well-established hallmark of cancer progression. This phenotypic transition is not driven by a single factor but is orchestrated by a symphony of signals from the TME including (1) soluble signaling molecules (e.g., *TGFβ, PDGF, FGF2*) and pro-inflammatory cytokines (e.g., *IL1A, IL6, TNFα*); (2) mechanical stress from the stiffened tumor matrix, which activates *YAP/TAZ* signaling; (3) metabolic reprogramming via lactate uptake (the "reverse Warburg effect"); and (4) hypoxia, which stabilizes *HIFs* and promotes expression of *VEGF* and ECM-modifying enzymes (*LOXL2*). Despite numerous pathways available for activation, our data clearly demonstrate that loss of rhythmicity of molecular clock, specifically *BMAL1* disruption is critical for this transition process. *LHX8* was identified among the top 10 most significantly upregulated genes in AM + AMF group. Importantly, genetic ablation of *BMAL1* in AMFs significantly abrogated both *LHX8* expression and the associated tumor-supportive phenotype, indicating that *BMAL1* is indispensable in this regulatory cascade. We observed that dysregulation of *BMAL1*—whether triggered by dysregulation of molecular clock, genetic modifications, or pharmacological intervention—might drive the transcriptional upregulation of *LHX8*, ultimately fostering a tumor-supportive niche. While the precise mechanistic network requires further investigation, these findings highlight the BMAL1-LHX8 axis as a central coordinator of stomal reprogramming in ameloblastoma. Additionally, the potential roles of the BMAL1-LHX8 axis in other *LHX8*-expressing stromal or neural crest-derived cellular microenvironments—possibly contributing to tumor progression across a broader range of malignancies—presents an intriguing avenue for future research. While the precise mechanisms through which this axis interacts with the broader signaling network remain unclear, our findings, combined with existing literature, support a compelling model: we propose that aberrant expression of *BMAL1* is an upstream initiator of AMF activation. *BMAL1* directly upregulates *LHX8* at the

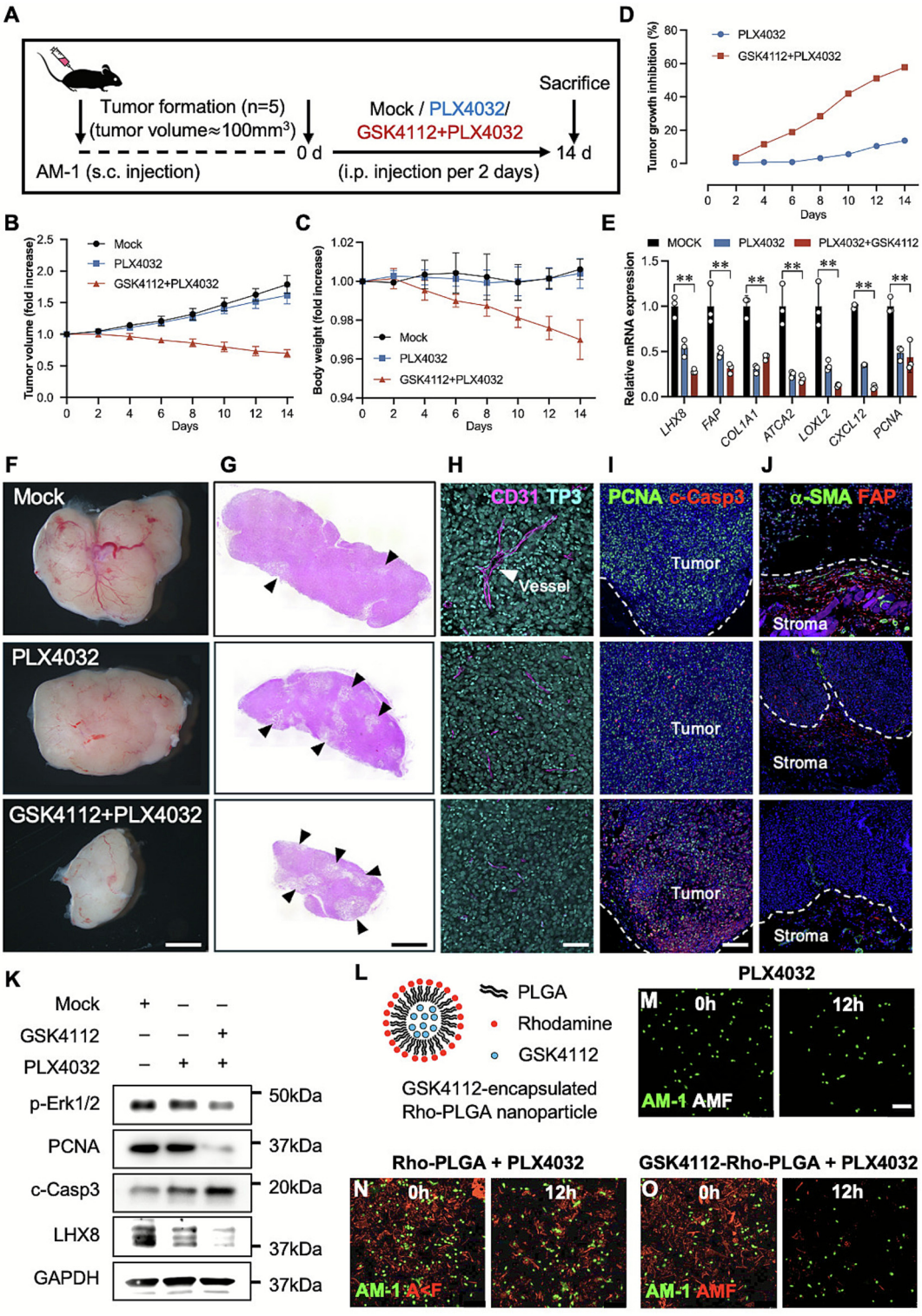

Fig. 6. GSK4112 elevate the sensitivity of ameloblastoma against vemurafenib *in-vivo* model. (A) Establishment of the AM-1 xenograft model and the experimental schedule. (B) The tumor volume was monitored every 2 days (during 14 days of experimental schedule). (C) Fold change in body weights of AM-1 xenograft mice. (D) Percentage of tumor growth inhibition (TGI). (E) Relative mRNA expression of *LHX8*, *FAP*, *COL1A1*, *ATCA2*, *LOXL2* and *CXCL12* in tumor mass that dissected from Mock, PLX4032 only and GSK4112 + PLX4032 administrated group. (F) Stereoscopic images for dissected tumor mass from each group. (G) H&E staining for paraffin section of dissected tumor mass. Arrowheads indicates apoptotic or necrotic areas. (H-J) Immunohistochemistry staining for CD31, PCNA, cleaved-caspase3, α-SMA and FAP. Dotted line indicates the interface between tumor mass and surrounding stromal tissue. Arrowheads indicates infiltrated blood vessels in the xenograft tumor mass. (K) Western blot assay for p-Erk1/2, PCNA, cleaved-caspase3, and LHX8 in each experimental group. (L) Structure of GSK4112-encapsulated Rho-PLGA nanoparticle. (M–O) Confocal images of AM-1 + AMF following PLX4032, Rho-PLGA + PLX4032, and GSK4112-Rho-PLGA + PLX4032 administration. Data were shown as mean ± SEM, one-way ANOVA followed Tukey's multiple comparisons test was used in B-E (B-C, n = 5, E, n = 3; $^{**}p < 0.01$). Scale bar: F and G, 1 mm; H, 50 μm; I and J, 100 μm; M–O, 200 μm. Nuclear stained with TO-PRO-3 (TP3).

transcriptional level, which in turn sensitizes fibroblasts to typical tumor-derived signals, facilitating a complete phenotypic transition and accounting for the concomitant upregulation of ECM and growth factor genes. Accordingly, elucidating these precise mechanistic relationships as a primary objective for our future work.

Our findings revealing a tumor-promoting function for *BMAL1* in AM, while contrasting with previous reports of its tumor-suppressive role in other tumors [12,43]. However, a growing body of evidence firmly establishes that the role of circadian clock genes in cancer is not universal but is highly context-dependent, influenced by factors such as tissue of origin, cell lineage, and the specific oncogenic drivers present [44]. Indeed, *BMAL1* can be co-opted by dominant oncogenic pathways, a phenomenon observed in glioblastoma [45] and leukemia stem cells [46], as well as in renal [47] and liver [48] carcinomas where *BMAL1* collaborates with factors like *HIF2α* to drive proliferation. This rewiring creates a therapeutic vulnerability through "non-oncogene addiction," rendering cancer cells uniquely dependent on *BMAL1*. We propose a similar mechanism in AM, where the local microenvironment and putative oncogenic signals, potentially from the MAPK pathway, have transformed *BMAL1* from a clock regulator into a crucial facilitator of tumor growth and its interaction with TME.

GSK4112 is a pioneering, first-in-class synthetic *REV-ERB* agonist that served as a vital chemical probe. It demonstrated potent agonist activity in biochemical and cellular assays, repressing core clock genes (e.g., *BMAL1*) and gluconeogenic genes in hepatocytes [49]. While SR9011 or SR9009 are optimized, second-generation *REV-ERB* agonists explicitly designed to provide sufficient plasma and brain exposure for *in-vivo* evaluation. A critical advantage of *REV-ERB* agonists is the wide therapeutic window: these compounds are only just metabolic regulators but also selectively lethal to cancer cells across a broad spectrum of tumor types, while sparing normal cells [50]. The most transformative innovation of this study is the utilization of circadian biology to 'normalize' the tumor-promoting stromal niche. Traditional therapies targeting CAFs encounter challenges due to cellular heterogeneity and toxicity. Here, we demonstrate that pharmacological inhibition of the BMAL1-LHX8 axis via GSK4112 shifts AMFs from an 'activated' to a 'quiescent' state. Of note, the localized delivery of GSK4112 using nanoparticles (e.g. PLGA) could mitigate the systemic effects on the host's central clock, thereby augmenting the efficacy of vemurafenib against ameloblastoma.

The probable mechanisms for addressing systemic toxicity via nanoparticle-based GSK4112 delivery are twofold: (1) Targeted delivery: Nanoparticles can be functionalized with ligands (e.g., against fibroblast activation protein) to achieve active targeting and selective accumulation within the stromal compartment of the tumor, thereby minimizing off-target effects on the central circadian pacemaker and healthy tissues. (2) Controlled release: Encapsulation in a nanoparticle platform allows for a sustained, localized release of the drug, which could be tuned to coincide with the peak activity of the BMAL1-LHX8 axis, aligning chronotherapy with precise drug delivery. This strategy would help confine the action of GSK4112 to the tumor microenvironment, thereby mitigating systemic exposure and potentiating a safer, more effective combination therapy with vemurafenib.

Several limitations should be considered: (1) Lack of single-cell resolution for tumor-AMF crosstalk. Our transcriptomic analysis captured bulk rhythmicity disruptions in stroma-rich tumoroids but could not provide real-time transcriptional dynamics during tumor-AMF interactions at single-cell level, potentially masking heterogenous AMF subpopulations driving dysregulation of molecular clock. (2) Incomplete mechanistic basis of the BMAL1-LHX8 network. While we established regulatory role of *BMAL1* over *LHX8* through knockdown studies and linked it to tumor-promoting functions such as ECM remodeling, growth factor secretion, we have yet to characterize the precise downstream effectors and direct transcriptional targets of *LHX8*. (3) Translational gaps in chronotherapy. Our GSK4112-loaded PLGA nanoparticles showed localized efficacy *in-vitro* but further validation at different Zeitgeber times *in-vivo* is necessary to evaluate long-term safety, central clock effects, and clinical scalability.

To sum up, the potent synergy we observed between the clock-modulator GSK4112 and vemurafenib provides a strong rationale for developing chronotherapeutic strategies for ameloblastoma and potentially other *BRAF*-mutant oral cancers. A key future challenge will be to determine the optimal timing for administering such circadian-targeting agents to coincide with the peak activity of the BMAL1-LHX8 pathway in the tumor stroma, thereby maximizing efficacy and minimizing off-target effects. This will require detailed chrono-pharmacological studies in pre-clinical models to map the daily oscillations of this axis. Furthermore, translating this to the clinic necessitates the development of reliable biomarkers, such as *LHX8* expression levels in biopsy samples, to identify patients most likely to benefit from this combination therapy. Ultimately, our work suggests that "stromal re-synchronization" could be a novel therapeutic principle, moving beyond direct tumor cell targeting to restore rhythmic homeostasis in the tumor microenvironment and overcome drug resistance.

Methods

Patient sample collection and criteria

Inclusion Criteria: Patients with a confirmed histopathological diagnosis of conventional ameloblastoma who underwent surgical resection at Department of Oral and Maxillofacial Surgery, Yonsei University College of Dentistry between 2022 and 2024, and from whom fresh-frozen or FFPE tissue was available with complete clinical data.

Exclusion Criteria: Patients with a history of prior radiotherapy or systemic therapy for ameloblastoma, those with insufficient tissue quality for analysis, or cases where informed consent was not obtained.

Cell culture and tumoroid formation

Keratinocyte serum-free medium (KSFM, 10724-011, Gibco, USA) supplemented with 2.5 μg Human Recombinant EGF (10450-013, Gibco, USA), 25 mg bovine pituitary extract (13028-014, Gibco, USA), and 1 % penicillin–streptomycin solution (15140163, Gibco, USA) was used for AM-1 culture according to the previous protocol [51]. All experiments involving primary cells were conducted using early-passage cells (P3–P5) obtained from a carefully selected group of seventeen independent patients with conventional ameloblastoma (patients' information was listed in Supplementary Table). The representative data presented in the figures were validated across at least three distinct patient-derived AMF lines, ensuring a thorough and comprehensive analysis. The isolation and culture of primary AM cell was followed by the previous method [24]. NFs and AMFs were cultured in Fibroblast Growth Medium (FGM-2, Cat# CC-3132). Growth medium consisting of Dulbecco's modified Eagle's medium (DMEM), 1 % penicillin–streptomycin solution, and 10 % fetal bovine serum was used for HEK293T, HUVEC, and HepG2 cell culture. All cells were incubated at 37 °C with 5 % CO2 and 95 % humidity.

For tumoroid formation, the primary AM cells were suspended in the ice cold Matrigel® (Standard concentration products, Corning, USA, 356255) and spotted on the 24-well dish (2.5×10^4 cells/spot) and grown in Advanced DMEM supplemented with

1 × B27, 1.25μmol/L N-acetyl-l-cysteine, 10μmol/L nicotinamide, 50 ng/mL human EGF, 500 nmol/L A83-01, 10 ng/mL human FGF10, 5 ng/mL human FGF2, 1 μmol/L prostaglandin E2, 0.3 μmol/L CHIR 99021, 1 μmol/L forskolin, 4 % R-spondin, and 4 % Noggin (R-spondin and Noggin were produced via the r-PEX protein expression platform at U-Protein Express BV), for 7 days. The AM tumoroids were used for co-cultured with normal fibroblasts (NFs)/ AMFs [52] Transwell® or establish the stroma-rich AM tumoroid.

To establish the stroma-rich AM tumoroid, 7-days-cultured AM tumoroids were mixed with NFs/ AMFs (5×10^4 cells) and plated into a U-bottom dish for 48 h (2:1 ratio of NFs/AMFs: AM tumoroids). The cell mixtures were re-embedded in Matrigel® and culture with co-culture medium (50:50, AM tumoroid medium and NF/AMF medium) for 14 days. The PLX4032 and GSK4112 was added into the growth medium and replaced every 2 days. The administration dose of PLX4032 (20 μM) was justified by toxicity test, whereas the dose for GSK4112 (10 μM) was adopted from the literature [53].

Animal

Fifteen immunocompromised male mice (post-natal 6 weeks, n = 15), with bodyweight around 25 g (BALB/C nu/nu purchased from Nara Biotech Co.), were utilized for the establishment of xenograft mice model. All mice were subcutaneously inoculated with 1×10^7 AM-1 cells on the left flank. Tumor volume was recorded every 2 days by measuring the longest (a) and shortest (b) tumor tissue diameters with a vernier caliper and calculated using the following formula: tumor volume = $0.5 \times a \times b^2$. When the tumor volume reached about 100 mm^3, the mice were randomly assigned to control (PBS), PLX4032, GSK4112 + PLX4032 groups (n = 5 per group) to minimize bias. Tumor-bearing mice received intravenous injections of Mock control, PLX4112, and GSK4112 + PLX4032 every 2 days. The administration dose of PLX4032 (100 mg/kg) was justified by toxicity test, whereas the dose of GSK4112 (100 mg/kg) was adopted from the literature [54]. Therapeutic agents were administered at a fixed Zeitgeber Time, specifically at Zeitgeber Time 16 (ZT16), where ZT0 is defined as the beginning of the light phase (lights-on), while investigators were not formally blinded during endpoint assessment and data collection. Tumor growth and body weight were monitored for 14d and fold-change in tumor volume and body weight were calculated by dividing the recorded value by the initial value. The percentage of tumor growth inhibition (TGI) was calculated by the following formula [55]: $TGI(\%) = 100\text{-}[(V/V_0)/(V_k/V_{k0}) \times 100]$, where V is the mean tumor volume in the treated group at the time point; V_0 is the mean tumor volume in the treated group at the initial time point; V_k is the mean tumor volume in the control group at the specific time point, and V_{k0} is mean tumor volume in the control group at the initial time point. Two weeks after administration, 15 mice (n = 5 per group) were euthanized for histological or molecular analysis.

Synchronization of circadian clock

The molecular rhythmicity in cells were synchronized by adding 100 nM dexamethasone to DMEM for 2 h, followed by replacement with basal medium. The time of replacement with the basal medium was designated as the circadian time (CT) of 0.

Construction and synthesis of the hBMAL1:Luc and hPER2::Luc reporter vector

pGL3-basis vector that contains cDNA encoding hLuc was obtained from Addgene (212936). The human PER2 (hPER2, 790 bp) promoter fragments were amplified by PCR reactions using specific primers (Supplementary Table). Enzymically cut the site between KpnI and BglII in pGL3-basis vector, and ligate the hPER2 into the linearized pGL3-basGis vector. Transform the ligated vector pGL3 [hPER2::Luc] to chemically competent *E. coli*. Amplify the selected *E. coli.* and extract DNA to get the hPER2::Luc vector.

Lentivirus production

HEK293T cells seeded in 100 cm^2 culture dishes and co-transfected with 10 μg packaging plasmid Pax2 and 5 μg envelope plasmid VSVG, and 10 μg hPER2::Luc vector. To harvest the lentiviral particles, the supernatant was centrifuged at 4100*g* for 30 min to remove cell debris and passed through a 45 μm filter. The lentiviral particles were stored at −80 °C.

Transduction with lentiviral vectors

For lentiviral transduction, cells (i.e., primary normal fibroblasts or cancer-associated fibroblasts) were seeded in 6-well plates and cultured for 24 h. On the day of transduction, 1 mL medium and 1 mL of lentiviral particles was added. A total of 8μg/mL protamine sulfate (Sigma-Aldrich, St. Louis, MO, USA) and 4 μg /mL polybrene (Sigma-Aldrich, St. Louis, MO, USA) was used to enhance transduction efficiency. The next day, the medium was replaced, and selection medium was added one day later (complete growth medium containing 100 μg /mL G418, Gibco, USA) to obtain stable transduced cells and incubated at 37 °C with 5 % CO_2 atmosphere.

Cell culture for bioluminescence measurements

Stable-transduced cell populations were selected and maintained in medium containing G418 (100 μg /mL, Gibco, USA). For bioluminescence evaluation, 20 μL of cell lysate and 100 μL of Luciferase Assay Reagent (LAR) were mixed and added in 96 well for measure the light produce in Luminometer and 250μM Luciferase assay reagent (LAR).

Preparation of Rhodamine-labeled GSK4112 encapsulated PLGA nanoparticles

Rhodamine-labeled PLGA nanoparticles encapsulating GSK4112 were fabricated using a modified double emulsion (W1/O/W2) solvent evaporation technique. In brief, 25 mg of PLGA (Corbion, Amsterdam, the Netherlands) and GSK4112 were dissolved in DCM, and 200 μL of TE buffer (pH 7.5; Sigma-Aldrich) was added to form the primary W1/O emulsion by probe sonication (UP100H, Hielscher Ultrasonics GmbH, Teltow, Germany). Subsequently, 2 mL of 2 % (w/v) PVA1500 solution was incorporated and sonicated again to yield a secondary W1/O/W2 emulsion. The emulsion was diluted with 6 mL of 2 % PVA1500 and magnetically stirred at room temperature for 3 h to allow solvent evaporation. The resulting nanoparticles were harvested by ultracentrifugation at 38,000*g* for 10 min at 4 °C (Optima Max, Beckman Coulter, Brea, CA, USA), washed twice with RNase-free deionized water, resuspended in water, and lyophilized. All types of PLGA nanoparticles were purchased from Nanoglia (Daejeon, Republic of Korea). The particle size and ζ-potential were determined using a Zetasizer Nano ZS (Malvern Instruments, Malvern, UK).

In-vitro administration of GSK4112-Rho-PLGA nanoparticle

The synthesis of PLGA nanoparticles and encapsulation of GSK4112 was performed by Nanoglia Inc. (Korea). CellTracker (Cat. C7025, USA, Invitrogen) stained AM-1 cells were co-cultured with AMFs in 6-well dish for 24 h, and followed by the

administration of PLX4032 (20 μM) or PLX4032 and GSK4112-Rho-PLGA under the guidance of instruction. The confocal image was captured at 12 h of post-administration.

Statistical analysis

All statistical analyses were performed using GraphPad Prism version 7.0. The ImageJ software was used to measure the percentage of positive cells (plugin: analyzed particles, size: 10–infinity, circularity: 0–1), intensity, and area. Differences were considered statistically significant at p-values of <0.05. All raw data used for quantitative analysis and plot generation in this study are provided in the Supplementary Table. The other methods that related to present study were described in detail in the Supplementary Materials.

Ethics approval and consent to participate

This study was approved by the institutional review board (IRB) at the University of Yonsei (2-20180050) and followed by human subject research guidelines and a protocol. Informed consent was obtained from all individual participants included in the study.

Data availability

The datasets used and/or analyzed during the current study are available from the corresponding author on reasonable request. The RNA sequencing data have been deposited in the Gene Express Omnibus (GEO) database [GEO: GSE279327].

Ethics approval and consent to participate

The animal experiments were conducted in compliance with the guidelines set by the Yonsei University Health System's Intramural Animal Care and Use Committee (YUHS-IACUC, No. 2020-1043). This study was approved from the institutional review board (IRB) at the University of Yonsei (2-20180050) and followed by human subject research guidelines and protocol. Informed consent was obtained from all individual participants included in the study.

Declaration of competing interest

The authors declare that they have no known competing financial interests or personal relationships that could have appeared to influence the work reported in this paper.

Acknowledgements

This study was supported by the Yonsei University College of Dentistry Fund (6-2023-0011).

Ethics approval and consent to participate

This study was approved by the institutional review board (IRB) at the University of Yonsei (2-20180050) and followed by human subject research guidelines and a protocol. Informed consent was obtained from all individual participants included in the study.

Appendix A. Supplementary data

Supplementary data to this article can be found online at https://doi.org/10.1016/j.jare.2025.11.069.

References

[1] Faden DL, Algazi A. Durable treatment of ameloblastoma with single agent BRAFi Re: Clinical and radiographic response with combined BRAF-targeted therapy in stage 4 ameloblastoma. J Natl Cancer Inst 2017;109. doi: https://doi.org/10.1093/jnci/djw190.
[2] Liu T, Zhou L, Xiao Y, Andl T, Zhang Y. BRAF inhibitors reprogram cancer-associated fibroblasts to drive matrix remodeling and therapeutic escape in melanoma. Cancer Res 2022;82:419–32. doi: https://doi.org/10.1158/0008-5472.CAN-21-0614.
[3] Li S, Lee DJ, Kim HY, Kim JY, Jung YS, Jung HS. Ameloblastoma modifies tumor microenvironment for enhancing invasiveness by altering collagen alignment. Histochem Cell Biol 2022;158:595–602. doi: https://doi.org/10.1007/s00418-022-02136-7.
[4] Liang C, Liu Z, Song M, Li W, Wu Z, Wang Z, et al. Stabilization of heterochromatin by CLOCK promotes stem cell rejuvenation and cartilage regeneration. Cell Res 2021;31:187–205. doi: https://doi.org/10.1038/s41422-020-0385-7.
[5] Reppert SM, Weaver DR. Coordination of circadian timing in mammals. Nature 2002;418:935–41. doi: https://doi.org/10.1038/nature00965.
[6] Xuan W, Khan F, James CD, Heimberger AB, Lesniak MS, Chen P. Circadian regulation of cancer cell and tumor microenvironment crosstalk. Trends Cell Biol 2021;31:940–50. doi: https://doi.org/10.1016/j.tcb.2021.06.008.
[7] Burgermeister E, Battaglin F, Eladly F, Wu W, Herweck F, Schulte N, et al. Aryl hydrocarbon receptor nuclear translocator-like (ARNTL/BMAL1) is associated with bevacizumab resistance in colorectal cancer via regulation of vascular endothelial growth factor a. EBioMedicine 2019;45:139–54. doi: https://doi.org/10.1016/j.ebiom.2019.07.004.
[8] Chen P, Hsu WH, Chang A, Tan Z, Lan Z, Zhou A, et al. Circadian regulator CLOCK recruits immune-suppressive microglia into the GBM tumor microenvironment. Cancer Discov 2020;10:371–81. doi: https://doi.org/10.1158/2159-8290.CD-19-0400.
[9] Yang Y, Yuan G, Xie H, Wei T, Zhu D, Cui J, et al. Circadian clock associates with tumor microenvironment in thoracic cancers. Aging (Albany NY) 2019;11:11814–28. doi: https://doi.org/10.18632/aging.102450.
[10] Zhao J, Zhou X, Tang Q, Yu R, Yu S, Long Y, et al. BMAL1 deficiency contributes to mandibular dysplasia by upregulating MMP3. Stem Cell Rep 2018;10:180–95. doi: https://doi.org/10.1016/j.stemcr.2017.11.017.
[11] Zheng L, Seon YJ, Mourao MA, Schnell S, Kim D, Harada H, et al. Circadian rhythms regulate amelogenesis. Bone 2013;55:158–65. doi: https://doi.org/10.1016/j.bone.2013.02.011.
[12] Tang Q, Cheng B, Xie M, Chen Y, Zhao J, Zhou X, et al. Circadian clock gene bmal1 inhibits tumorigenesis and increases paclitaxel sensitivity in tongue squamous cell carcinoma. Cancer Res 2017;77:532–44. doi: https://doi.org/10.1158/0008-5472.CAN-16-1322.
[13] Shan L, Zheng W, Bai B, Hu J, Lv Y, Chen K, et al. BMAL1 promotes colorectal cancer cell migration and invasion through ERK- and JNK-dependent c-Myc expression. Cancer Med 2023;12:4472–85. doi: https://doi.org/10.1002/cam4.5129.
[14] Wang X, Jiang W, Pan K, Tao L, Zhu Y. Melatonin induces RAW264.7 cell apoptosis via the BMAL1/ROS/MAPK-p38 pathway to improve postmenopausal osteoporosis. Bone Joint Res 2023;12:677–90. doi: https://doi.org/10.1302/2046-3758.1211.BJR-2022-0425.R3.
[15] Zhou C, Yang G, Chen M, Wang C, He L, Xiang L, et al. Lhx8 mediated Wnt and TGFbeta pathways in tooth development and regeneration. Biomaterials 2015;63:35–46. doi: https://doi.org/10.1016/j.biomaterials.2015.06.004.
[16] Flandin P, Zhao Y, Vogt D, Jeong J, Long J, Potter G, et al. Lhx6 and Lhx8 coordinately induce neuronal expression of Shh that controls the generation of interneuron progenitors. Neuron 2011;70:939–50. doi: https://doi.org/10.1016/j.neuron.2011.04.020.
[17] Niu W, Spradling AC. Mouse oocytes develop in cysts with the help of nurse cells. Cell 2022;185(2576–2590):e2512.
[18] Zhou C, Yang G, Chen M, He L, Xiang L, Ricupero C, et al. Lhx6 and Lhx8: cell fate regulators and beyond. FASEB J 2015;29:4083–91. doi: https://doi.org/10.1096/fj.14-267500.
[19] Zhao Y, Guo YJ, Tomac AC, Taylor NR, Grinberg A, Lee EJ, et al. Isolated cleft palate in mice with a targeted mutation of the LIM homeobox gene lhx8. PNAS 1999;96:15002–6. doi: https://doi.org/10.1073/pnas.96.26.15002.
[20] Tomioka T, Shimazaki T, Yamauchi T, Oki T, Ohgoh M, Okano H. LIM homeobox 8 (Lhx8) is a key regulator of the cholinergic neuronal function via a tropomyosin receptor kinase a (TrkA)-mediated positive feedback loop. J Biol Chem 2014;289:1000–10. doi: https://doi.org/10.1074/jbc.M113.494385.
[21] van den Helder R, Steenbergen RDM, van Splunter AP, Mom CH, Tjiong MY, Martin I, et al. HPV and DNA methylation testing in urine for cervical intraepithelial neoplasia and cervical cancer detection. Clin Cancer Res 2022;28:2061–8. doi: https://doi.org/10.1158/1078-0432.CCR-21-3710.
[22] Kim JY, Jeon SH, Park JY, Suh JD, Choung PH. Comparative study of LHX8 expression between odontoma and dental tissue-derived stem cells. J Oral Pathol Med 2011;40:250–6. doi: https://doi.org/10.1111/j.1600-0714.2010.00970.x.
[23] Ferrari N, Ranftl R, Chicherova I, Slaven ND, Moeendarbary E, Farrugia AJ, et al. Dickkopf-3 links HSF1 and YAP/TAZ signalling to control aggressive behaviours in cancer-associated fibroblasts. Nat Commun 2019;10:130. doi: https://doi.org/10.1038/s41467-018-07987-0.

[24] Li S, Lee DJ, Kim HY, Kim JY, Jung YS, Jung HS. Unraveled roles of Cav1.2 in proliferation and stemness of ameloblastoma. Cell Biosci 2022;12:145. doi: https://doi.org/10.1186/s13578-022-00873-9.
[25] Valera PS, Plou J, Garcia I, Astobiza I, Viera C, Martin JE, Sasselli IR, Carracedo A, Liz-Marzan LM. SERS analysis of cancer cell-secreted purines reveals a unique paracrine crosstalk in MTAP-deficient tumors. PNAS 2023;120:e2311674120. doi: https://doi.org/10.1073/pnas.2311674120.
[26] Altemus MA, Goo LE, Little AC, Yates JA, Cheriyan HG, Wu ZF, et al. Breast cancers utilize hypoxic glycogen stores via PYGB, the brain isoform of glycogen phosphorylase, to promote metastatic phenotypes. PLoS One 2019;14: e0220973. doi: https://doi.org/10.1371/journal.pone.0220973.
[27] Wang Z, Han G, Liu Q, Zhang W, Wang J. Silencing of PYGB suppresses growth and promotes the apoptosis of prostate cancer cells via the NF kappaB/Nrf2 signaling pathway. Mol Med Rep 2018;18:3800–8. doi: https://doi.org/10.3892/mmr.2018.9388.
[28] Xiao L, Wang W, Huangfu Q, Tao H, Zhang J. PYGB facilitates cell proliferation and invasiveness in non-small cell lung cancer by activating the Wnt-beta-catenin signaling pathway. Biochem Cell Biol 2020;98:565–74. doi: https://doi.org/10.1139/bcb-2019-0445.
[29] Zhou Y, Jin Z, Wang C. Glycogen phosphorylase B promotes ovarian cancer progression via Wnt/beta-catenin signaling and is regulated by miR-133a-3p. Biomed Pharmacother 2019;120:109449. doi: https://doi.org/10.1016/j.biopha.2019.109449.
[30] Eun JW, Yoon JH, Ahn HR, Kim S, Kim YB, Lim SB, et al. Cancer-associated fibroblast-derived secreted phosphoprotein 1 contributes to resistance of hepatocellular carcinoma to sorafenib and lenvatinib. Cancer Commun (Lond) 2023;43:455–79. doi: https://doi.org/10.1002/cac2.12414.
[31] Qi R, Bai Y, Li K, Liu N, Xu Y, Dal E, et al. Cancer-associated fibroblasts suppress ferroptosis and induce gemcitabine resistance in pancreatic cancer cells by secreting exosome-derived ACSL4-targeting miRNAs. Drug Resist Updat 2023;68:100960. doi: https://doi.org/10.1016/j.drup.2023.100960.
[32] Zhang H, Deng T, Liu R, Ning T, Yang H, Liu D, et al. CAF secreted miR-522 suppresses ferroptosis and promotes acquired chemo-resistance in gastric cancer. Mol Cancer 2020;19:43. doi: https://doi.org/10.1186/s12943-020-01168-8.
[33] Kim S, Li S, Jangid AK, Park HW, Lee DJ, Jung HS, et al. Surface engineering of natural killer cells with CD44-targeting ligands for augmented cancer immunotherapy. Small 2024;20:e2306738. doi: https://doi.org/10.1002/smll.202306738.
[34] Davidson S, Efremova M, Riedel A, Mahata B, Pramanik J, Huuhtanen J, et al. Single-cell RNA sequencing reveals a dynamic stromal niche that supports tumor growth. Cell Rep 2020;31:107628. doi: https://doi.org/10.1016/j.celrep.2020.107628.
[35] Chang TH, Shanti RM, Liang Y, Zeng J, Shi S, Alawi F, et al. LGR5(+) epithelial tumor stem-like cells generate a 3D-organoid model for ameloblastoma. Cell Death Dis 2020;11:338. doi: https://doi.org/10.1038/s41419-020-2560-7.
[36] Stone LD, Massicano AVF, Stevens TM, Warram JM, Morlandt AB, Lapi SE, et al. (89)Zr-panitumumab PET imaging for preoperative assessment of ameloblastoma in a PDX model. Sci Rep 2022;12:19187. doi: https://doi.org/10.1038/s41598-022-23531-z.
[37] Altman BJ, Hsieh AL, Sengupta A, Krishnanaiah SY, Stine ZE, Walton ZE, et al. MYC disrupts the circadian clock and metabolism in cancer cells. Cell Metab 2015;22:1009–19. doi: https://doi.org/10.1016/j.cmet.2015.09.003.
[38] Relogio A, Thomas P, Medina-Perez P, Reischl S, Bervoets S, Gloc E, et al. Ras-mediated deregulation of the circadian clock in cancer. PLoS Genet 2014;10: e1004338. doi: https://doi.org/10.1371/journal.pgen.1004338.
[39] Lee Y, Lahens NF, Zhang S, Bedont J, Field JM, Sehgal A. G1/S cell cycle regulators mediate effects of circadian dysregulation on tumor growth and provide targets for timed anticancer treatment. PLoS Biol 2019;17:e3000228. doi: https://doi.org/10.1371/journal.pbio.3000228.
[40] Aiello I, Fedele MLM, Roman F, Marpegan L, Caldart C, Chiesa JJ, et al. Circadian disruption promotes tumor-immune microenvironment remodeling favoring tumor cell proliferation. Sci Adv 2020;6. doi: https://doi.org/10.1126/sciadv.aaz4530.
[41] Gutierrez-Monreal MA, Trevino V, Moreno-Cuevas JE, Scott SP. Identification of circadian-related gene expression profiles in entrained breast cancer cell lines. Chronobiol Int 2016;33:392–405. doi: https://doi.org/10.3109/07420528.2016.1152976.
[42] Kiessling S, Beaulieu-Laroche L, Blum ID, Landgraf D, Welsh DK, Storch KF, et al. Enhancing circadian clock function in cancer cells inhibits tumor growth. BMC Biol 2017;15:13. doi: https://doi.org/10.1186/s12915-017-0349-7.
[43] Wu J, Jing X, Du Q, Sun X, Holgersson K, Gao J, et al. Disruption of the clock component Bmal1 in mice promotes cancer metastasis through the PAI-1-TGF-beta-myoCAF-dependent mechanism. Adv Sci (Weinh) 2023;10:e2301505. doi: https://doi.org/10.1002/advs.202301505.
[44] Battaglin F, Chan P, Pan Y, Soni S, Qu M, Spiller ER, et al. Clocking cancer: the circadian clock as a target in cancer therapy. Oncogene 2021;40:3187–200. doi: https://doi.org/10.1038/s41388-021-01778-6.
[45] Xuan W, Hsu WH, Khan F, Dunterman M, Pang L, Wainwright DA, et al. Circadian regulator CLOCK drives immunosuppression in glioblastoma. Cancer Immunol Res 2022;10:770–84. doi: https://doi.org/10.1158/2326-6066.CIR-21-0559.
[46] Puram RV, Kowalczyk MS, de Boer CG, Schneider RK, Miller PG, McConkey M, et al. Core circadian clock genes regulate leukemia stem cells in AML. Cell 2016;165:303–16. doi: https://doi.org/10.1016/j.cell.2016.03.015.
[47] Mello RM, Gomez Ceballos D, Sandate CR, Wang S, Jouffe C, Agudelo D, et al. BMAL1 and ARNT enable circadian HIF2alpha responses in clear cell renal cell carcinoma. Nat Commun 2025;16:5834. doi: https://doi.org/10.1038/s41467-025-60904-0.
[48] Qu M, Zhang G, Qu H, Vu A, Wu R, Tsukamoto H, et al. Circadian regulator BMAL1::CLOCK promotes cell proliferation in hepatocellular carcinoma by controlling apoptosis and cell cycle. PNAS 2023;120:e2214829120. doi: https://doi.org/10.1073/pnas.2214829120.
[49] Grant D, Yin L, Collins JL, Parks DJ, Orband-Miller LA, Wisely GB, et al. GSK4112, a small molecule chemical probe for the cell biology of the nuclear heme receptor Rev-erbalpha. ACS Chem Biol 2010;5:925–32. doi: https://doi.org/10.1021/cb100141y.
[50] Sulli G, Rommel A, Wang X, Kolar MJ, Puca F, Saghatelian A, et al. Pharmacological activation of REV-ERBs is lethal in cancer and oncogene-induced senescence. Nature 2018;553:351–5. doi: https://doi.org/10.1038/nature25170.
[51] Li S, Lee DJ, Kim HY, Harada H, Jung YS, Jung HS. Transcriptomic comparison analysis between ameloblastoma and AM-1 cell line. Int J Stem Cells 2022;15:415–21. doi: https://doi.org/10.15283/ijsc22132.
[52] Sharpe BP, Nazlamova LA, Tse C, Johnston DA, Thomas J, Blyth R, et al. Patient-derived tumor organoid and fibroblast assembloid models for interrogation of the tumor microenvironment in esophageal adenocarcinoma. Cell Rep Methods 2024;4:100909. doi: https://doi.org/10.1016/j.crmeth.2024.100909.
[53] Wang Q, Sundar IK, Lucas JH, Park JG, Nogales A, Martinez-Sobrido L, et al. Circadian clock molecule REV-ERBalpha regulates lung fibrotic progression through collagen stabilization. Nat Commun 2023;14:1295. doi: https://doi.org/10.1038/s41467-023-36896-0.
[54] Solt LA, Wang Y, Banerjee S, Hughes T, Kojetin DJ, Lundasen T, et al. Regulation of circadian behaviour and metabolism by synthetic REV-ERB agonists. Nature 2012;485:62–8. doi: https://doi.org/10.1038/nature11030.
[55] Alexander RK, Liou YH, Knudsen NH, Starost KA, Xu C, Hyde AL, et al. Bmal1 integrates mitochondrial metabolism and macrophage activation. Elife 2020;9. doi: https://doi.org/10.7554/eLife.54090.